NEW CONCEPT OF COMBINED HYDRO-THERMAL RESPONSE TESTS (H/TRTS) FOR GROUND HEAT EXCHANGERS

Jean Rouleau[a], Louis Gosselin[a*], Jasmin Raymond[b]

[a]Department of Mechanical Engineering, Université Laval, Quebec City, QC, Canada
[b]Institut National de la Recherche Scientifique – Centre Eau Terre Environnement (INRS-ETE), Quebec City, QC, Canada

Article accepté pour publication dans : Geothermics, Volume 62, Juillet 2016

Abstract

Current thermal response tests, used to estimate the subsurface thermal conductivity in the geothermal domain, are not designed to take into account groundwater flows. To measure the flow parameters, a new concept has been developed. Heating cables are installed within a borehole in contact to the formation, with three temperature probes strategically located at the edge of the borehole. Study of the evolution of temperature for each probe during both a heat injection phase and a recovery period allows determining ground thermal conductivity, groundwater flow velocity and orientation. Numerical simulations have been used to validate the proposed concept and establish its limits.

Keywords: geothermal; groundwater; ground heat exchanger; thermal response test; thermal conductivity.

Nomenclature

A, B	Correlation parameter [-]
E	Error, [-] or [%]
Fo	Fourier number [-]
f	Dimensionless vector function [-]
P	Pressure [Pa]

[*] Corresponding author: Louis.Gosselin@gmc.ulaval.ca; Tel.:+1-418-656-7829; Fax: +1-418-656-5343.

Pe	Peclet number [-]
T	Temperature [K, °C]
c_p	Thermal capacity [J/kg K]
k	Thermal conductivity [W/mK]
q_0'	Borehole heat transfer rate per unit length [W/m]
L	Required borefield length [m]
r	Radial coordinate [m]
t	Time [s]
u	Velocity [m/s]
x,y	Cartesian coordinates [m]

Greek symbols

α	Thermal diffusivity, [m^2/s]
θ	Relative temperature $T-T_g$, [K, °C]
β, ϕ	Angle [°]
κ	Ground permeability [m^2]
μ	Dynamic viscosity [$Pa \cdot s$]
ρ	Density [kg/m^3]
η	Ground porosity [-]
τ	Pulse time [year, month, hour]
σ	Ratio of volumetric thermal capacity [-]

Subscripts

avg	Average
b	Borehole
c	Critical
D	Darcy
eff	Effective
f	Fluid
g	Undisturbed ground

L	Lowest
U	Uniform
H	Heating Period
h	Hourly pulse
M	Monthly pulse
max	Maximum
min	Minimum
s	Solid
y	Yearly pulse
0	Initial

Symbols

~	Non-dimensional
$\rightarrow$	Vector

1. Introduction

The increasing demand for clean energy and the growing concerns over global warming and emissions of CO_2 have led to a regain of interest for green energies. Over the last decades, the use of ground-coupled heat pump (GCHP) systems has developed fast. The number of units installed per year in Canada has grown by a factor close to 1 000% between 2000 and 2010 [1]. GCHP systems transfer heat to the ground (or from the ground) for space heating or cooling in residential and commercial buildings. For a good sizing of borehole heat exchangers (BHEs), engineers need to properly estimate the thermal properties of the ground. Thermal conductivity is an essential parameter in order to characterize the heat transfer between a ground heat exchanger and the surrounding subsurface. Thermal response tests (TRTs) are used for in situ measurement of the subsurface thermal properties. In a typical TRT, the evolution of the temperature of the water circulating in the BHE is measured at the inlet and outlet of the BHE. Then, using Kelvin's line source theory, which is based on Fourier's law of conduction, or based on other models to represent heat transfer around the borehole, it is possible to deduce the ground thermal properties [2][3][4][5][6]. Kelvin's line source model assumes an infinite,

homogenous and isotropic ground in which heat transport in the ground is completely driven by conduction [7].

Unfortunately, the assumptions on which this model relies can turn out to be false. One of the most significant limitations is the lack of consideration of convective heat transfer in the ground. Geothermal borefields can be installed in aquifers. If the geological materials is sufficiently permeable or submitted to a strong hydraulic gradient, groundwater will move through the ground pores or fractures, which affects heat transfer around BHEs [8][9][10]. Since the line source model neglects groundwater flows, it has been shown that TRTs in such cases can provide wrong estimates of the subsurface thermal conductivity [5][11][12][13], and most importantly, oversizing of the BHEs. Advection enhances heat transfer between the BHE and the subsurface, which means that shorter BHEs than in the absence of groundwater flow can be installed to satisfy the same load. Analytical [14] and numerical [15][16][17][18] models were established to simulate heat transfer around a BHE with groundwater flow. Nevertheless, current TRTs do not provide information on the hydrogeological information required to size the borefield, namely groundwater velocity and direction.

Accounting for groundwater flows is primordial when designing GCHP systems [19]. In recent works, it has been demonstrated that neglecting groundwater flow in design procedure can induce an overdesign of the borefield length that can go up to 68% [20]. Engineers not only need to consider groundwater flowrate, but the direction of the flow is also an important parameter [21]. These parameters have to be known when applying adequate models for the design of geothermal borefield. Determining such parameters requires hydrogeological tests which might be prohibitive in terms of time and cost when designing and installing a GCHP system. Therefore, there is a need to develop a combined hydrogeological and thermal test to acquire the required estimates of ground properties in the design process.

Another possible point of improvement to current TRTs is to obtain a subsurface thermal conductivity profile instead of an average value. Other alternative tests have been proposed to obtain a profile of the ground properties, with the use of optical fibers [22][23][24] or thermostratigraphy [25]. However, these methods are either highly

expensive or require the knowledge of additional data such as the local geothermal gradient.

In this paper, we address some of the shortcomings mentioned above by developing a configuration of combined hydro-thermal response tests (H/TRT). This H/TRT is inspired by the work of Raymond [26][27], in which a heating cable is placed in a borehole to inject heat in the subsurface during the TRT. Theoretically, with multiple temperature probes positioned in a horizontal plane around the cable, it is possible to observe the strength and direction of groundwater flow. Using heating cable sections to directly generate heat in the borehole requires less power than conventional TRT and less equipment. It is also possible to obtain a vertical profile of the ground thermal conductivity if the test is simultaneously accomplished at various depths. Continuous heating cables can also be used, but require high tension to provide enough heat.

The objective behind this paper is to use numerical simulations to validate the potential of the concept before performing field experiments. The first part of the paper details the concept and the numerical model that was built to simulate its performance in various possible geological cases. Results are then shown in the following sections. From these results, a methodology is proposed to accurately estimate the subsurface thermal conductivity and groundwater flow parameters.

2. Description of the concept

Based on the work of Raymond et al. [26], the proposed concept of H/TRT uses a heating cable placed in a borehole to inject heat in the subsurface. This strategy to inject heat in the borehole has already been numerically validated for the measurement of thermal conductivity [27] and yielded promising results based on in situ testing in U-tube ground heat exchangers [28]. In the present paper, however, the heating cable is installed directly in the "empty" borehole (not in the U-tube) that is in contact with the formation. Moreover, groundwater flows have not been considered thus far in that type of tests, hence the need for an adaptation to account for them. In order to do so, it is proposed to use three temperature sensors (instead of one) to measure the evolution of the temperature in the borehole during the heat injection from the source. These probes are distributed uniformly on the edge of the well (i.e., at an interval of 120 degrees). The cable is positioned at the

center of the hole. Since the heat plume generated by the source is deformed in the direction of the groundwater flow, each sensor will monitor different temperature evolutions. Therefore, by comparing every sensor measurement, one could potentially estimate the ground thermal conductivity, along with the groundwater flow parameters (i.e., velocity and orientation). The test is performed in a borehole before it is filled with grout. The proposed setup is sketched in Fig. 1.

The idea behind the H/TRT is similar to that employed by hydrogeologists measuring the hydraulic head at three different wells to determine groundwater flow velocity and direction [29]. The differences are that temperature is the variable measured instead of the hydraulic head, and the test is performed in a single well. In order to constrain the measurement of groundwater flow parameters within a single well, hydrogeologists can also employ a heat-pulse groundwater flow meter, which uses a similar approach to the proposed H/TRT, but cannot provide estimation of the ground thermal conductivity [30]. Lee and Lam proposed a test where they monitored three concurrent standard TRTs in three adjacent boreholes [31]. Other ways of obtaining hydraulic characterization from temperature data have been suggested in the past [32][33]. Simultaneous TRTs and well tests executed in a single borehole greatly reduce both the duration of the test and the equipment needed. However, it is important to note that the estimation of groundwater flow properties within a single well provides localized results. In a heterogeneous ground, it remains preferable to evaluate these properties from three boreholes to get an average value over a larger area.

In the present H/TRT, it is proposed to record the probes temperature for a certain period of heating (e.g., three days), followed by a recovery period (no heating) of equivalent duration. The exact position of the sensors and of the heat source might not be precisely known, which can lead to uncertainties on the measured ground properties. It was found that the recovery period can help to reduce these potential errors since the temperature field tends to become more uniform during recovery [34].

3. Mathematical and numerical models

Numerical simulations have been performed in order to establish the potential of the H/TRT approach presented in Section 2. Numerical models are fairly easy-to-use and offer

the possibility of measuring precisely the individual impacts of various parameters, such as the subsurface thermal conductivity or the groundwater flow rate. Heat transfer in the presence of groundwater flow is a complex process that combines both conduction and advection. The finite element method (FE) has been used to simulate heat transfer and groundwater flow.

Readers are referred again to Fig. 1 to see the numerical domain. It consists of a borehole of radius r_b embedded in a saturated porous medium. Dry ground is seen as the matrix of the porous medium and its pores are filled with water (saturated ground). To verify the concept in the most favorable situation, no tube casing was input in the model, resulting in a permeable boundary between the borehole and the saturated ground. In a non-rocky soil, a tube casing might be necessary to prevent collapse of the borehole. In such cases, the casing induces an impermeable borehole-ground boundary and the groundwater flow cannot go into the borehole. Although this makes it more difficult to observe the impact of groundwater flow, the H/TRT is expected to carry out similar results. Table 1 offers typical values of thermal and hydraulic properties for different geological materials, assuming a hydraulic gradient of 0.001 m/m [35]. While properties for dry ground were consistently modified between each simulation, properties of water used by the model remained fixed and are given in Table 2. Preliminary simulations showed that groundwater flow had a negligible impact on TRT for flows with Darcy velocity inferior to 10^{-8} m/s, hence properties of silt and clay were not considered in this study. Materials are assumed to be isotropic. Dimensions of the numerical domain were normalized by the borehole radius – its length was 85 times longer than the radius of the borehole while its height was 42.5 times larger. The borehole radius length varied between $r_b = 0.05\,\mathrm{m}$ and $r_b = 0.1\,\mathrm{m}$ depending on the simulation case.

3.1 Governing equations

The physical laws governing the problem are the conservation of mass, momentum and energy. In order to limit the computational time, the domain was approximated as two-dimensional. The first two laws are considered in the Navier-Stokes equation, modified to

take into account the porous medium. Since the velocity and pressure fields were assumed not to change with time, a steady-state version of the equations was considered:

$$\rho \nabla \cdot \underline{u} = 0 \tag{1}$$

$$\frac{\rho}{\eta}\left((\underline{u} \cdot \nabla)\frac{\underline{u}}{\eta} \right) = \nabla \cdot \left(-P + \frac{\mu}{\eta}\left(\nabla \underline{u} + (\nabla \underline{u})^{T} \right) \right) - \frac{\mu}{\kappa}\underline{u} \tag{2}$$

This formulation has the advantage that it is valid both in the ground (porous media with a finite value for the permeability) and in the well itself (where the last term of Eq. (2) vanishes). Therefore, the same set of equations can be solved in the entire domain. Far from the borehole, an easy way to approximate the average groundwater flow velocity is to use the Darcy's velocity:

$$u_{r\to\infty} \equiv u_D = -\frac{\kappa_g}{\mu}\frac{\partial P}{\partial x} \tag{3}$$

The conservation of energy equation must include both conduction and advection. In a porous medium, it reads as

$$(\rho c_p)_f \left(\sigma \frac{\partial \theta}{\partial t} + \underline{u} \cdot \nabla \theta \right) = \nabla \cdot (k_{avg} \nabla \theta) \tag{4}$$

where:

$$\theta = T - T_g \quad , \quad \sigma = \frac{\eta (\rho c_p)_f + (1-\eta)(\rho c_p)_s}{(\rho c_p)_f} \tag{5}$$

Note that the index "avg" for k is to indicate the average ground thermal conductivity around the borehole. The values of thermal conductivity and thermal diffusivity depend on the porosity of the ground matrix:

$$k_{avg} = \eta k_f + (1-\eta) k_s \quad , \quad \alpha_{avg} \equiv \frac{k_{avg}}{(\rho c_p)_f} \tag{6}$$

Again, the advantage of Eq. (4) is that it can be used in the entire domain. In the well, there is only water and no dry ground, meaning that for that part of the domain, conservation of energy is represented by:

$$(\rho c_p)_f \left(\frac{\partial \theta}{\partial t} + \underline{u} \cdot \nabla \theta \right) = \nabla \cdot (k_f \nabla \theta) \tag{7}$$

In order to limit the number of variables, the problem was solved with dimensionless variables:

$$x^* y^* \equiv \frac{x, y}{r_b}, \quad \vec{u}^* \equiv \frac{\vec{u} r_b}{\alpha_{eff}}, \mathrm{Pe} \equiv \frac{u_D r_b}{\alpha_{avg}}, \quad \mathrm{Fo} \equiv \frac{t\alpha_{avg}}{r_b^2},$$
$$\theta^* \equiv \frac{2\pi k_{avg} \theta}{q_0'}, \quad k^* \equiv \frac{k_{avg}}{k_w} \quad \text{and} \quad P^* \equiv \frac{P\kappa_g}{\mu\alpha_f} \tag{8}$$

Here, q_0' presents the heat injection rate of the source during the heating process. The ground effective volumetric heat capacity has to be known for the calculations of Fo and Pe. According to [36], the volumetric heat capacity can be estimated solely based on the identification of the host rock where the borehole is drilled with an uncertainty of $\pm 15\%$. Based on the data from Tables 1 and 2, ranges employed for each dimensionless scales can be seen in Table 3. The velocity vector can be expressed as a product between the Peclet number Pe and a dimensionless vector function:

$$\vec{u}^*(x^*, y^*) = \mathrm{Pe} \cdot \vec{f}(x^*, y^*) \tag{9}$$

Using these scales, Eqs. (4) and (7) can be reduced to:

$$\sigma \frac{\partial \theta^*}{\partial \mathrm{Fo}} + \mathrm{Pe} \cdot \vec{f}(x^*, y^*) \cdot \nabla^* \theta^* = k^* \nabla^{*2} \theta^* \tag{10}$$

$$\frac{\partial \theta^*}{\partial \mathrm{Fo}} + \mathrm{Pe} \cdot \vec{f}(x^*, y^*) \cdot \nabla^* \theta^* = \nabla^{*2} \theta^* \tag{11}$$

The entire domain is initially at $\theta^* = 0$. Far from the borehole, the temperature of the boundaries is fixed at the initial value. A pressure gradient is imposed to generate the groundwater flow. While the value of P^* at the left boundary varies according to the desired groundwater velocity, the dimensionless pressure of the right side remains $P^* = 0$ for all simulations. This means that groundwater flows in the numerical domain from left to right.

In developing this model, the following assumptions were made:

(i) Local thermal equilibrium is assumed, i.e. water and ground temperatures are the same locally;

(ii) Groundwater flow is assumed to be unidirectional and parallel to the ground surface. Furthermore, groundwater flow is supposed to be present everywhere in the aquifer and to be stationary over the duration of the test;

(iii) The heat transfer is also assumed to be parallel to the ground surface. This assumption is fairly good considering the short periods of time over which tests are performed [37].

(iv) All properties are assumed to be uniform and non-affected by temperature;

(v) Dispersivity is not considered explicitly in the model. Although some models account for it [13][35][38], few data is available for quantifying thermal dispersion of typical groundwater flows.

(vi) Natural convection inside the well is neglected. It has been proved that for TRT using heating cable, natural convection can be greatly limited with perforated disks positioned at strategic vertical positions to cut off possible circulating loops [27]. Tests based on the heat-pulse groundwater flow meter usually limits natural convection with the use of packers. Executing the test with continuous heat cable also minimize natural convection if the setup is properly done [39].

3.2 Numerical model

To solve numerically the above-mentioned differential equations within the domain, a commercial finite element software was used [40]. The mesh generated has unstructured triangular elements that are concentrated around the borehole, where high temperature gradients are expected due to the presence of the heat source. Considering the symmetry of the domain, only half of the domain needs to be simulated. An infinite element zone that was 8.5 time longer than the radius of the borehole was added to the model boundary. It was verified that the domain dimensions had no effect on the simulation results, i.e. that when a larger domain is used, the results stay the same. Time stepping needed to solve the

energy equation is automatically chosen by the software during simulation, adjusted with a relative tolerance of 10^{-3}.

To ensure the correctness of the results, mesh convergence was verified. The mesh independence was considered to be reached when doubling the number of elements in the domain yielded a relative discrepancy of less than 1% on the average probes temperature for every time-step in the considered range. The mesh independence study was performed with groundwater flowing far from the borehole at a Peclet number of $\mathrm{Pe} = 0$ and $\mathrm{Pe} = 0.1$. For typical values of $\alpha_{eff} = 10^{-6}\,\mathrm{m}^2/\mathrm{s}$ and $r_b = 0.075\mathrm{m}$, a Peclet number of 0.1 translates to a Darcy velocity of $u_D = 1.33 \cdot 10^{-6}\,\mathrm{m/s}$. These correspond to extreme parameter values, hence the chosen mesh can be applied to every simulation cases if it works for these. The final mesh that was used for simulations contained 7,944 elements.

4. Influence of groundwater flow during H/TRT

In order to assess the heat transfer mechanisms during the H/TRT proposed in this paper, numerical simulations were carried out. Simulations were performed to evaluate the impacts of advection on the thermal response of the system. Simulations did not account for variations of σ as there is a limited range of possible values for this parameter in typical permeable geological materials. A value of $\sigma = 0.6$ was considered for all simulations.

To observe the impact of groundwater flows during the suggested TRT concept, the thermal response created by the heat source was simulated for multiple values of the Peclet number (Pe). Although the influence of advection on the transient evolution of a borehole average temperature has been investigated before, the distribution of temperature produced within the borehole by groundwater flows has received considerably less attention. Fig. 2 offers a view of the distribution of temperature in the borehole for a flow of $\mathrm{Pe} = 0.1$, after a day of heating. A ratio of thermal conductivities of $k = 4$ and a power input of 40 W/m for the heat source were used. The center of the borehole, where the cable is positioned, is clearly the warmest area of the domain. The white lines, which represent isothermal lines, are not axisymmetric around the heat source – they are pushed towards the flow orientation, which is represented by the arrow in Fig. 2. Therefore, temperature at

different positions along the borehole perimeter should read different temperatures. This is confirmed by Fig. 3, which presents the thermal response at seven positions along the borehole perimeter at an increment of 30 degrees for four distinct values of Pe. A dimensionless duration of $\mathrm{Fo} = 50$ was used for the heating period. The influence of groundwater flow can easily be seen when comparing the curves of Fig. 3. Because the heat plume generated by the source stretches in the direction of the flow, sensors that are aligned with the groundwater flow read higher temperatures than the ones that are opposite to the flow, thus creating a difference of temperatures between the sensors. This difference of temperatures widens as Pe increases. In the case of $\mathrm{Pe} = 0.1$, the gap of temperature between sensors is higher than 1°C during most of the heating period, making it possible to notice the influence of subsurface flow. Again, such a Peclet number can easily be reached with a Darcy velocity of $u_D \sim 10^{-6}\,\mathrm{m/s}$. On the other hand, the curves for $\mathrm{Pe} = 0.01$ are similar to the thermal response of the purely conductive case. As a result, with a heat injection rate of 40 W/m, it appears that the setup cannot properly detect advection at such a low Peclet number value.

As expected, for all Pe values, during the recovery stage, differences of temperature quickly vanish as temperature in the borehole becomes uniform in a short period of time. A uniform temperature in the borehole can be beneficial because of the evaluation the thermal conductivity becomes less sensitive to the exact position of the cable and sensors within the borehole. Additionally, since the borehole itself is included in the radius of influence of the H/TRT around the heating cable during the injection phase, and since the borehole is filled only by water (which has a low thermal conductivity), a thermal conductivity determined during the heating phase would tend to underestimate the ground thermal conductivity. During the recovery phase, the uniform temperature in the water fixes this issue as there is no heat transfer in the borehole itself.

Concerning the differences of temperature between the sensors, it was found that they build up quickly in the early stage of the heating period $(\mathrm{Fo} < 10)$. Rapidly, despite of the fact that no steady-state condition is reached, the differences of temperature follow a nearly-constant evolution and progress slowly. In other words, the temperature increases at the same pace for all sensors. This pattern was the same for all Pe as presented in Fig. 4.

It shows the difference of temperature between the sensor reading the highest temperature and the six other probes.

As for the calculation of thermal conductivity, unless water flows at an extreme velocity, the effective ground thermal conductivity measured by a TRT should be nearly equal to the true thermal conductivity [10]. Eqs. (10) and (11) show that advection effects increase with time and thus, advection may not be important enough to alter the measurements of TRTs considering their relatively short duration. To verify this, simulations of 3 days of heating in different geological environments were done after which the ground thermal conductivity was calculated from the line source method. Table 4 shows that within the range of Peclet studied in this paper (≤ 0.1), the line source method provides approximately the same value of thermal conductivity for all flow velocities. The effective thermal conductivity changed only when $\mathrm{Pe} > 0.1$, which is out of the scope of this work. Nevertheless, the evaluation of the groundwater flows parameters is important for a good borefield design as long-term performance of the heat exchangers is strongly influence by the flow [41].

5. Proposed methodology for H/TRT analysis

Section 4 has shown the impact of groundwater flow during the thermal response of the H/TRT setup. The object of the H/TRT is to determine three main parameters: the ground effective thermal conductivity, the groundwater flow velocity and orientation. By evaluating properly the thermal response, it could be possible to isolate the impact of each of these parameters and then to estimate their values. Here, a method to do so will be developed.

5.1 Evaluation of the groundwater flow orientation

Since the determination of the flow orientation does not require a particular knowledge of ground properties and is helpful for the estimation of Pe, it is suggested to start the analysis there. A methodology similar to that used in hydrogeology is proposed to find the orientation of the groundwater flow from an H/TRT. In hydrogeology, the path of a subsurface flow is found by locating the equipotential lines. Equipotential lines are the

lines where the hydraulic head remains constant. Since the motion of water is strictly driven by the hydraulic gradient, the flow has to be perpendicular to such lines in an isotropic medium. Therefore, if the hydraulic head is known at three different horizontal positions, it is possible to interpolate the direction of equipotential lines and thus to know the orientation of the flow. Although this method is relatively precise, it has the disadvantage that it requires three boreholes to be drilled.

Here, instead of the hydraulic head, it is the temperature that is measured at three distinct positions within a single borehole. This means that the suggested setup cannot directly determine equipotential lines, but it allows users to identify the isothermal lines, hence a similar approach can be used. The direction of the flow was estimated to be the parallel to the gradient of the plane formed by the temperature values measured at the three sensor points. Since advection carries the heat generated by the source in the flow direction, the heat plume described by isothermal lines should be parallel to the motion of groundwater (Fig. 2). Simulations were performed to verify this hypothesis and assess the measurement error on the flow direction adopting this method, for different values of Pe. Table 5 shows the outcome of this investigation, which was done with $k_s/k_g = 4$ and a heat rate of 40 W/m. It shows the flow direction determined from the isotherms compared to the actual orientations, for three cases. This study was repeated for different ratios of conductivities, and the results were similar as will be shown later. To correctly represent real thermal sensors, temperatures calculated with the numerical model were rounded to the nearest tenth. In most cases when $Pe < 0.005$, the setup is not sensitive to groundwater flow and therefore the orientation measurement was impracticable. However, the impact of the groundwater flow on the heat transfer between the borehole and the ground is negligible for these values of Darcy velocity, and therefore, for the sizing of boreholes, this data is actually not that useful. In other words, the knowledge of the flow orientation is not vital at low Pe numbers. When Pe is higher, the error on the measurement was found to be inferior to 15°. The method was more effective for a flow of $Pe = 0.05$ than a flow of $Pe = 0.1$. This is caused by the fact that the heat plume generated by the source becomes narrower for great velocities. Sensors located outside of the plume are not affected by the heat source which can lead to wrong estimate of the orientation. The temperature measurements were taken at the end of the heating stage in this study.

5.2 Evaluation of groundwater flow velocity

Referring back to Figs. 3 and 4, it can be seen that the main effect of the groundwater flow velocity is to increase the differences of temperature measured by the sensors on the periphery of the borehole. This increase happens during the early stage of the heating period and the differences of temperature are nearly constant later. Accordingly, the maximal difference of temperature on the borehole perimeter ΔT_{max} appears to be essentially proportional to the flow velocity. As shown in Fig. 5, ΔT_{max} is defined as the difference of temperature between two sensors on the borehole perimeter that would be aligned in the direction of the flow, i.e. one upstream and one downstream. In practice, if the flow orientation ϕ is known and a gap of temperatures is sensed between each sensor, a trigonometric calculation gives a good approximation of ΔT_{max} via extrapolation:

$$\begin{aligned} T_{max} &= T_H + (T_H - T_L)\frac{1-\cos\beta}{\cos\beta - \cos(\beta+120°)} \\ T_{min} &= T_L - (T_H - T_L)\frac{1-\cos(\beta+120°)}{\cos\beta - \cos(\beta+120°)} \\ \Delta T_{max} &= T_{max} - T_{min} \end{aligned} \tag{12}$$

Eqs. (12) assumes that the temperature field in the borehole can be approximated by a plane. Note that the angle β used in Eq. (12) is not necessary equal to ϕ - ϕ is the angle between the flow orientation and a reference x-axis and β is the angle between the flow and the sensor with the highest temperature value, which is not necessarily along the reference axis. To reduce the number of variables, ΔT_{max} has been translated into a dimensionless parameter:

$$\Delta T^{\%}_{max} = \frac{k_w \Delta T_{max}}{q'_0} \tag{13}$$

Eqs. (12) shows that the extrapolation of $\Delta T^{\%}_{max}$ depends on the value of the flow orientation taken into account by the angle β. As a result, the accuracy of the extrapolation is

influenced by the evaluation of β. Table 6 shows how dependent the determination of $\Delta\tilde{T}_{max}$ is to the flow orientation. For the sake of illustration, the test was done with $\tilde{k}=4$ and Pe = 0.05 at a flow orientation of $\phi = 30°$. $\Delta\tilde{T}_{max}$ was calculated at Fo = 50. Other sets of parameters were also considered with similar results. The table shows that Eqs. (12) provide a satisfying estimate of $\Delta\tilde{T}_{max}$ even when β is not precisely known. When the error on the flow orientation evaluation is lower than ±20°, extrapolating $\Delta\tilde{T}_{max}$ with Eqs. (12) leads to accurate results (errors smaller than 10%).

Since the value of $\Delta\tilde{T}_{max}$ evolves with time, it was decided to evaluate it at a given Fourier number. Doing so, the only remaining independent variables are Pe and the ratio of thermal conductivities. Fig. 6 shows the evolution of $\Delta\tilde{T}_{max}$ according to these two parameters. Data were extracted at a dimensionless time of $\mathrm{Fo} = 10$ during the heating stage. This Fourier value was chosen because it was observed that the difference of temperature between sensors changes slowly for $\mathrm{Fo} > 10$. Fig. 6 reveals that one can find the subsurface flow Peclet number as long as the difference of temperature is large enough since $\Delta\tilde{T}_{max}$ is nearly linearly dependent on Pe. $\tilde{k}$ merely changes the slope of the line function between Pe and $\Delta\tilde{T}_{max}$. Its impact is only observable for high values of Pe $\left(\text{i.e. } \mathrm{Pe} \geq 0.02\right)$, but neglecting the ratio of conductivities can lead to error that are up to 20% when $\mathrm{Pe} \approx 0.1$ and thus must not be completely ignored.

5.3 Evaluation of thermal conductivity

The ground thermal conductivity can be estimated during the recovery period by curve-fitting the evolution of the average borehole wall temperature $\bar{\theta}_b\left(\mathrm{Fo}\right)$ calculated by a model to the one that is observed in the borehole temperature once it becomes uniform. To do that, it is approximated that the average temperature of the borehole wall is equal to the mean value of the three thermal sensors. Calculated temperature evolution can be obtained using a dimensionless ground function $G\left(\mathrm{Fo}\right)$, that is used to determine the temperature increment during heat injection:

$$\bar{\theta}_b(\mathrm{Fo}) = \frac{q'_0}{k_{eff}} G(\mathrm{Fo}) \quad (14)$$

Once heat injection is stopped, the temporal superposition principle can be used to calculate $\bar{\theta}_b(\mathrm{Fo})$:

$$\bar{\theta}_b(\mathrm{Fo}) = \frac{q'_0}{k_{eff}} \left(G(\mathrm{Fo}) - G(\mathrm{Fo} - \mathrm{Fo}_H) \right) \quad (15)$$

where Fo_H is the Fourier number when heat injection is stopped.

5.3.1 Time needed for the temperature in the borehole to be uniform

Simulations were carried out to provide an estimation of the dimensionless time required to reach temperature uniformity in the borehole Fo_U once the heat source is turned off. The temperature uniformity criterion was arbitrarily set at 0.1°C everywhere in the borehole. Uniformity of temperature within the borehole is not necessarily reached when all three sensors have the same reading as the middle of the borehole could be warmer due to presence of the heat source. To circumvent this problem, it is possible to place a fourth sensor near the source to directly find the moment when the temperature is uniform or the results presented here can be used to get an estimate. The simulations showed that there is a logarithmic relation between Fo_H and Fo_U:

$$\mathrm{Fo}_U = q'_0 \left(A \ln(\mathrm{Fo}_H) + B \right) \quad (16)$$

where A and B are functions of Pe and k_{ratio}. Table 7 provides the values of A and B for different sets of Pe and k_{ratio}. The time required for the temperature to become uniform during thermal recovery increases for fast flows, but remains relatively short for grounds with high thermal conductivity. The value of Fo_U can be estimated either from calculations done during the heating period or from regional data. In most cases, it is smaller than Fo_H.

5.3.2 Ground function for various Pe and k_{ratio}

Advection not only leads to different temperatures read by each sensor, it also alters the temporal development of the mean temperature value of these sensors. A high k_{ratio} value

means that the subsurface has a high thermal conductivity compared to the one in the borehole and as a result, heat quickly travels out of the borehole area. Thus the ratio of thermal conductivities also affects the mean temperature value of the borehole perimeter. From Eq. (14), this implies that the G-function has to be adapted with Pe and $\tilde{k}$. This subsection offers a tool to estimate $G(\mathrm{Fo})$. Fig. 7 presents $G(\mathrm{Fo})$ for different values of Pe and of $\tilde{k}$, directly given by the numerical model. For short time-scales, while Pe has no effect on the G-function, $G(\mathrm{Fo})$ is highly influenced by $\tilde{k}$. The impact of $\tilde{k}$ is only observable for $\mathrm{Fo} < 10$. Then, for longer time scales, advection comes in and the groundwater flow starts to dominate the heat transfer process over radial conduction. The critical Fourier Fo_c separating these two states highly depends on Pe. While $\mathrm{Fo}_c \approx 10$ for flows of $\mathrm{Pe} = 0.1$, this value increases up to $\mathrm{Fo}_c \approx 250$ when $\mathrm{Pe} = 0.025$. These critical values can be used to determine the limit of the pure conductive stage if one wants to use the line-source theory to deduce the effective thermal conductivity during the heating period. In spite of the presence of groundwater flows, typical TRT durations are not long enough for the system to reach a steady-state, unless the test is executed in an unusually high permeable aquifer $(\mathrm{Pe} > 0.1)$. With the dimensionless time range used for this analysis, effects of convection on the G-function become apparent when $\mathrm{Pe} \geq 0.02$. Not accounting for advection during TRT analysis leads to erroneous estimation of thermal conductivity when the flow Darcy velocity is higher than this value.

5.4 Schematic step-by-step analysis procedure

Fig. 8 presents a summary of the suggested analysis method in a step-by-step procedure. After the preliminary steps of choosing test parameters, the H/TRT can be executed and then analysed. As previously explained, it is relatively easy to quickly obtain a good estimate for the groundwater flow orientation ϕ from the H/TRT data. Once this evaluation is done, it is possible to extrapolate the dimensionless maximum difference of temperature $\Delta\tilde{T}_{max}$ on the borehole perimeter using trigonometry. This dimensionless parameter is linked to the flow velocity number and thus could be used to obtain the Peclet number.

However, the relation between $\Delta T'_{max}$ and Pe is affected by the ratio of thermal conductivities k', which is still unknown. Therefore, an iterative procedure is required and a guess has to be made on the ground effective thermal conductivity k_{avg}. This guess on k_{avg} allows users to convert time values into Fourier numbers Fo and to measure a temporary value for Pe. Following that, curve-fitting on $G(Fo)$ is needed to get a new value for the ground thermal conductivity. It is preferable to do this curve-fitting when the temperature in the borehole is uniform during thermal recovery since it decreases the impact of an erroneous position for the heat source or the sensors due to the absence of heat transfer within the borehole. To find when the temperature in the borehole is uniform, a fourth sensor can be placed within the borehole or Table 7 along with Eq. (16) can be used. If the curve for the average borehole wall temperature observed in the field fits with the one calculated with $G(Fo)$, then the iterative process is complete and the values for Pe and k' are final. If not, another iteration is required, going back to the calculation of Pe.

The procedure was numerically tested for numerous situations. To mimic a resolution of 0.1 °C for the temperature sensors, numerical data were rounded to the nearest tenth. Fig. 9 shows the results of 25 H/TRT tests with different orders of magniture for k' and Pe. The values for k', Pe, ϕ, q'_0, r_b and t_H where randomly selected, but had to fit within a realistic range (Table 3). No more than three iterations were required for each test.

Thermal conductivity values determined by this procedure were all within a range of 10% of the input value in the numerical model. The methodology has a tendency to underestimate the ground thermal conductivity because of the presence of the borehole which is only filled with water – the fluid thermal conductivity is lower than the ground thermal conductivity, hence the slight underestimation. Measurements for the Darcy velocity were accurate when $u_D > 10^{-7}\,m/s$ as the measurement error was under $\pm 10\%$ for all situations involving such a flow. Below that value of u_D, measurements yielded less precise results. The H/TRT might be unable to reveal the groundwater flow when it is too weak. Fortunately, for geothermal applications, it is not needed to know the groundwater flowrate with great accuracy in that range of Darcy velocity. Simply knowing that the flow

is weak is good enough for sizing vertical heat exchangers when the velocity is small. Evaluations of the flow orientation were relatively accurate when $u_D > 10^{-7}\,m/s$. For slower groundwater flow, the direction estimation methodology is less effective. Obviously, the angle cannot be estimated when the setup cannot sense groundwater flow.

To assess the impact of the errors on the hydro-thermal ground parameters estimated from the above-mentioned H/TRT procedure, the overdesign of the borefield total length produced by these errors were determined using a spreadsheet that considers groundwater flow for the calculation of required length of geothermal borefield L [20]. Calculations were done using typical values of borefield characteristics (Table 8). The total BHE length was calculated both with input values (i.e. values considered as the right or real ones) of ground thermal conductivity, groundwater flow velocity and orientation and with their estimations (i.e., that obtained from the test). The required lengths calculated with both sets of values (i.e. real values versus those obtained from the test) were very similar. The borefield overdesign was more than 10% for only one simulation case, mostly because of a poor choice for the test parameters – the power input for the heating period, which only lasted 40 hours, was 20 W/m for that specific test. With proper test parameters (i.e. higher heat generation rate and longer heating period), the borefield overdesign is not critical and thus the H/TRT seem to offer a good tool for sizing geothermal borefields. For the heat injection rate, according to results, a power input superior to 30 W/m seems sufficient if the temperature probes have a resolution of 0.1°C. As for the duration of the heating period, a period longer than $Fo > 10$ is recommended to get a large difference of temperature between the sensors. Considering a minimal thermal conductivity of the ground around 1 W/mK and a maximal volumetric heat capacity close to 3×10^6 J/m^{3}K, the minimal ground thermal diffusivity is approximately $\alpha \approx 3.33\times10^{-7}\,m^2/s$. This means that, in a borehole with a radius of $r_b = 0.075m$, the heat source has to be activated for at least 46 hours to be sure that the minimal Fourier number is reached.

Until now, the uncertainties related to the position of the heat source and temperature sensors were not included in the analyses. Earlier, it was explained that the measurement of thermal conductivity is not affected by these errors as it is estimated during the recovery period, when the borehole temperature is uniform. However, a misplacement

of the source and the sensors can lead to inaccurate estimates of groundwater flow properties. Additional simulations were performed to assess the order of magnitude of these errors. In a first series of simulations, the source was placed at the mid-position between the center of the borehole and its edge. It was found that when the source misplacement is towards the flow orientation, the proposed methodology overrates the groundwater flow velocity. As the source is closer to the edge of the borehole, it is easier for the heat generated to reach the ground and leave the borehole, as if water was flowing at a faster pace. When the shift is perfectly aligned with the flow orientation, it nearly doubles the groundwater flow velocity measurement. On the other hand, a source dephasing that goes against the flow will lead to an underrated evaluation. The underrating of the groundwater flow velocity can go up top 70%. As for the measurement of flow orientation, the misplacement of the source only causes errors of $\pm 15°$. No correlation was found between the angular misplacement of the source and the magnitude of the flow orientation measurement error.

As for the position of the temperature sensors, the influence of their misplacement on the measurement of groundwater flow velocity is minimal provided that they remain equidistantly positioned on the circumference of the borehole. The error on the flow direction is equal to the misplacement of the equidistantly positioned sensors. It was shown before that the evaluation of the velocity is based on the extrapolation of the maximal difference of temperature on the borehole perimeter. Table 6 provides an error of about 15% on this extrapolation assuming a 30° error on the flow orientation. Thus, a misplacement of 30° on the sensors still gives satisfying measurements on the groundwater flow properties. A more extensive sensitive analysis where various combinations of source and sensors positions will be required in the future.

6. Conclusions

This paper introduced a new configuration of H/TRT to simultaneously estimate the ground thermal and hydraulic properties. The setup uses three temperature sensors set around a heating cable in a borehole. Evolution of temperature is monitored by all sensors during both the heating period and the thermal recovery. A numerical model was used to evaluate the potential of the concept. With the help of tools given in the paper, the thermal responses

of each sensor reveal the subsurface effective thermal conductivity, the groundwater flow velocity and its orientation. Knowing the flow properties is important for designing appropriate geothermal borefields. Since the tools provided are based on dimensionless scales, they offer flexibility regarding the heat injection rate, the duration of the heating period and the borehole dimensions. The amount of energy required by the TRT procedure does not exceed what is actually used by conventional TRTs. Moreover, the method is highly adaptable as it works for low power sources in geological settings that have low hydraulic conductivity. It is possible to execute it at various depths to find the distribution of ground properties, leading to better designs.

Numerical simulations were done to reproduce the heat transfer produced by the TRT for various conditions. Variations of the ground thermal conductivity, the groundwater flow velocity and orientation, the heat injection rate, the borehole radius and the duration of the heating period were considered for numerical validation of the system. Simulations disclosed that, in spite of the presence of advection, it is possible to deduce thermal conductivity by curve fitting the thermal response during thermal recovery. It is suggested to calculate thermal conductivity during the recovery. As for the parameters of the groundwater flow, they are estimated during the heating stage because they are measured via the differences of temperatures between the sensors. These gaps of temperatures are higher when the heat source is on. The creation of differences of temperatures that are perceptible can be achieved with a power source of 60 W/m unless the flow is small enough to be neglected in the heat transfer process. However, for low Peclet numbers, it is possible that the setup is unable to sense any flow. Since thermal recovery is monitored, the total duration of the test might be higher than conventional TRTs.

The numerical model built for this study was 2D. Three-dimensional effects accounting for natural convection or geothermal temperature gradient could be investigated in future work. An additional work would be to establish the number of vertical measurements that would be needed in order to obtain a satisfactory vertical distribution of ground and groundwater flow properties. The model used a permeable boundary between the ground and the borehole, hence it does not consider the borehole thermal resistance, contrarily to traditional TRTs. Furthermore, an extensive sensitivity analysis of

the variables, such as the position of the heat source and sensors, or the thermal properties for groundwater, would be helpful as there are many high uncertainties when working with ground properties. The suggested concept also needs to be tested in-situ and experimentally validated.

This work demonstrates the potential of the proposed TRT to reveal thermal and hydraulic ground properties while keeping the time, cost and equipment low. Development of thermal response tests accounting for groundwater flow should be pursued in the future to enhance the designing of geothermal borefields.

Acknowledgements

This work was supported by the Fond de recherche du Québec sur la nature et les technologies (FRQNT).

References

[1] Canadian GeoExchange Coalition, “The State of the Canadian Geothermal Heat Pump Industry 2011, Industry Survey and Market Analysis.” 2012.

[2] P. Mogensen, “Fluid fo duct wall heat transfer in duct system heat storages,” presented at the International Conference on Subsurface Heat Storage in Theory and Practice, Stockholm, Sweden, 1983, pp. 652–657.

[3] S. Gehlin, “Thermal Response Test method development and evaluation,” Doctoral Thesis, Lulea University of Technology, Lulea, Sweden, 2002.

[4] B. Sanner, G. Hellström, J. Spitler, and S. Gehlin, “Thermal response test–current status and world-wide application,” in *Proceedings world geothermal congress*, 2005, pp. 24–29.

[5] S. Signorelli, S. Bassetti, D. Pahud, and T. Kohl, “Numerical evaluation of thermal response tests,” *Geothermics*, vol. 36, no. 2, pp. 141–166, Apr. 2007.

[6] H. J. L. Witte, “TRT: How to get the right number,” *GeoDrilling Int.*, vol. 151, pp. 30–34, Apr. 2009.

[7] H. S. Carslaw and J. C. Jaeger, *Conduction of Heat in Solids*, Second Edition. Clarendon Press, Oxford, 1959.

[8] M. G. Sutton, D. W. Nutter, and R. J. Couvillion, “A Ground Resistance for Vertical Bore Heat Exchangers With Groundwater Flow,” *Journal of Energy Resources Technology*, p. 183, 2003.

[9] N. Diao, Q. Li, and Z. Fang, “Heat transfer in ground heat exchangers with groundwater advection,” *Int. J. Therm. Sci.*, vol. 43, no. 12, pp. 1203–1211, Dec. 2004.

[10] A. D. Chiasson, S. J. Rees, and J. D. Spitler, “A preliminary assessment of the effects of groundwater flow on closed-loop ground source heat pump systems,” *ASHRAE Trans.*, vol. 106, no. 1, pp. 380–393, 2000.

[11] H. J. L. Witte and G. J. Gelder, “Geothermal response tests using controlled multipower level heating and cooling around a borehole heat exchanger,” presented at the Proceedings of the Tenth Internation Conference on Thermal Energy Storage, New Jersey, USA, 2006.

[12] S. E. A. Gehlin and G. Hellström, “Influence on thermal response test by groundwater flow in vertical fractures in hard rock,” *Renew. Energy*, vol. 28, no. 14, pp. 2221–2238, Nov. 2003.
[13] J. Raymond, R. Therrien, L. Gosselin, and R. Lefebvre, “Numerical analysis of thermal response tests with a groundwater flow and heat transfer model,” *Renew. Energy*, vol. 36, no. 1, pp. 315–324, Jan. 2011.
[14] N. Molina-Giraldo, P. Blum, K. Zhu, P. Bayer, and Z. Fang, “A moving finite line source model to simulate borehole heat exchangers with groundwater advection,” *Int. J. Therm. Sci.*, vol. 50, no. 12, pp. 2506–2513, Dec. 2011.
[15] A. Angelotti, L. Alberti, I. La Licata, and M. Antelmi, “Energy performance and thermal impact of a Borehole Heat Exchanger in a sandy aquifer: Influence of the groundwater velocity,” *Energy Convers. Manag.*, vol. 77, pp. 700–708, Jan. 2014.
[16] R. Fan, Y. Jiang, Y. Yao, D. Shiming, and Z. Ma, “A study on the performance of a geothermal heat exchanger under coupled heat conduction and groundwater advection,” *Energy*, vol. 32, no. 11, pp. 2199–2209, Nov. 2007.
[17] Y. Nam, R. Ooka, and S. Hwang, “Development of a numerical model to predict heat exchange rates for a ground-source heat pump system,” *Energy Build.*, vol. 40, no. 12, pp. 2133–2140, 2008.
[18] J. C. Choi, J. Park, and S. R. Lee, “Numerical evaluation of the effects of groundwater flow on borehole heat exchanger arrays,” *Renew. Energy*, vol. 52, pp. 230–240, Apr. 2013.
[19] A. Chiasson and A. O’Connell, “New analytical solution for sizing vertical borehole ground heat exchangers in environments with significant groundwater flow: Parameter estimation from thermal response test data,” *Hvacampr Res.*, vol. 17, no. 6, pp. 1000–1011, 2011.
[20] M. Tye-Gingras and L. Gosselin, “Adapting design procedure for vertical ground heat exchangers to consider groundwater flow,” *Renewable Energy (submitted)*.
[21] C. K. Lee and H. N. Lam, “Effects of groundwater flow direction on performance of ground heat exchanger borefield in geothermal heat pump systems using 3-D finite difference method,” in *Proceedings of Building Simulation*, 2007, pp. 337–341.
[22] J. Acuña, P. Mogensen, and B. Palm, “Distributed thermal response test on a U-pipe borehole heat exchanger,” in *Effstock-The 11th International Conference on Energy Storage. Stockholm*, 2009.
[23] H. Fujii, H. Okubo, M. Chono, M. Sasada, S. Takasugi, and M. Tateno, “Application of optical fiber thermometers in thermal response tests for detailed geological descriptions,” in *Proceedings of Effstock 2009 conference on thermal energy storage for efficiency and sustainability, Stockholm, Sweden*, 2009.
[24] H. Fujii, H. Okubo, K. Nishi, R. Itoi, K. Ohyama, and K. Shibata, “An improved thermal response test for U-tube ground heat exchanger based on optical fiber thermometers,” *Geothermics*, vol. 38, no. 4, pp. 399–406, Dec. 2009.
[25] A. E. Beck, “The use of thermal resistivity logs in stratigraphic correlation,” *Geophysics*, vol. 41, no. 2, pp. 300–309, Apr. 1976.
[26] J. Raymond, G. Robert, R. Therrien, and L. Gosselin, “A novel thermal response test using heating cables,” in *Proceedings of the World Geothermal Congress, Bali, Indonesia*, 2010, pp. 1–8.
[27] J. Raymond and L. Lamarche, “Development and numerical validation of a novel thermal response test with a low power source,” *Geothermics*, vol. 51, no. 0, pp. 434–444, Jul. 2014.

[28] J. Raymond, L. Lamarche, and M. Malo, “Insights from field experiments to conduct thermal response tests with a low power source,” presented at the Proceedings of the 11th Internation Energy Agency Heat Pump Conference, Montréal, 2014, p. 12.
[29] N. Kresic, *Hydrogeology and groundwater modeling*, Second Edition. Taylor & Francis Group, 2007.
[30] A. S. Alden and C. L. Munster, “Field Test of the in situ permeable ground water flow sensor,” *Ground Water Monitoring and Remediation*, pp. 81–88, 1997.
[31] H. N. Lam and C. K. Lee, “Determination of groundwater flow direction in thermal response test analysis for geothermal heat pump systems,” *HVACampR Res.*, vol. 17, pp. 991–999, 2011.
[32] V. Wagner, P. Bayer, G. Bisch, M. Kübert, and P. Blum, “Hydraulic characterization of aquifers by thermal response testing: Validation by large-scale tank and field experiments,” *Water Resour. Res.*, vol. 50, no. 1, pp. 71–85, Jan. 2014.
[33] H. R. Bravo, F. Jiang, and R. J. Hunt, “Using groundwater temperature data to constrain parameter estimation in a groundwater flow model of a wetland system,” *Water Resour. Res.*, vol. 38, no. 8, pp. 28–1, Aug. 2002.
[34] J. Raymond, R. Therrien, and L. Gosselin, “Borehole temperature evolution during thermal response tests,” *Geothermics*, vol. 40, no. 1, pp. 69–78, Mar. 2011.
[35] N. Molina-Giraldo, P. Bayer, and P. Blum, “Evaluating the influence of thermal dispersion on temperature plumes from geothermal systems using analytical solutions,” *Int. J. Therm. Sci.*, vol. 50, no. 7, pp. 1223–1231, Jul. 2011.
[36] H. J. L. Witte, “Error analysis of thermal response tests,” *Appl. Energy*, vol. 109, pp. 302–311, Sep. 2013.
[37] P. Eskilson, “Thermal Analysis of Heat Extraction Boreholes,” Ph.D. Thesis, Lund University, Lund, Sweden, 1987.
[38] V. Wagner, P. Bayer, M. Kübert, and P. Blum, “Numerical sensitivity study of thermal response tests,” *Renew. Energy*, vol. 41, pp. 245–253, May 2012.
[39] S. M. H. Moghaddam and J. H. Barman, “First step towards development of distributed thermal response test using heating cables,” Kungliga Tekniska högskolan, Stockholm, 2015.
[40] COMSOL, *COMSOL Multiphysics User’s Guide, Version 4.2*. Stockholm, Sweden.
[41] E. Zanchini, S. Lazzari, and A. Priarone, “Long-term performance of large borehole heat exchanger fields with unbalanced seasonal loads and groundwater flow,” *Energy*, vol. 38, no. 1, pp. 66–77, Feb. 2012.
[42] T. L. Bergman, A. S. Lavine, F. P. Incropera, and D. P. DeWitt, *Fundamentals of heat and mass transfer*, Seventh. John Wiley & Sons, 2011.

Table 1. Typical groundwater Darcy velocity in various geological materials [35].

Aquifer materials	**Hydraulic conductivity [m/s]**	**Darcy velocity* U_D [m/s]**	**Thermal conductivity k_{avg} [W/mK]**	**Volumetric heat capacity ρC_p [10 MJ/m^{3}K]**
Gravel	10^{-4}-10^{-2}	10^{-7}-10^{-5}	1.8	2.4
Coarse sand	10^{-3}	10^{-6}	1.7-5.0	2.2-2.9
Medium sand	10^{-4}	10^{-7}	1.7-5.0	2.2-2.9
Fine sand	10^{-6}-10^{-5}	10^{-9}-10^{-8}	1.7-5.0	2.2-2.9
Silt	10^{-7}	10^{-10}	0.9-2.3	1.6-3.4
Clay	10^{-10}-10^{-9}	10^{-13}-10^{-12}	1.2-1.5	2.3

* Assuming hydraulic gradient of 0.001 m/m

Table 2. Properties of water for the numerical model [42].

Properties	**Value**
ρ_w [kg/m^3]	999
μ_w [kg/ms]	$1.08 \cdot 10^{-3}$
k_w [W/mK]	0.598
$c_{p,w}$ [J/kgK]	4 184

Table 3. Simulated range for all variables.

Variable	**Values tested**
Pe	10^{-3} to 10^{-1}
Fo	0 to 1 000
σ	0.55 to 0.75
ρ	2 to 8

Table 4. Effective thermal conductivity calculated from the line source method for different flow velocities.

Peclet number Pe [-]	**Measured effective thermal conductivity k_{eff} [W/mK]**
0.001	4.58
0.005	4.58
0.01	4.58
0.05	4.59
0.1	4.62
0.5	6.40

Table 5. Direction calculated after a day of heating for different groundwater velocities.

Peclet number Pe [-]	**Calculated direction $(\phi_{true} = 70°)$ [°]**	**Calculated direction $(\phi_{true} = 147°)$ [°]**	**Calculated direction $(\phi_{true} = 271°)$ [°]**
0.005	60.0	138.2	270.0
0.01	74.5	145.2	263.1
0.05	72.5	143.1	268.4
0.1	76.0	140.8	265.4

Table 6. Error on the extrapolation of the maximal difference of temperature calculated with Eq. (12) according to the accuracy of the flow orientation measurement ($\Delta\tilde{\gamma}_{\max,\text{true}} = 3.78\times10^{-2}$)

Error on β [°]	$\Delta\tilde{\gamma}_{\max,\text{calculated}}$ **[10^{-2}]**	**Relative error on $\Delta\tilde{\gamma}_{\max}$ [%]**
0	3.78	0.00
5	3.79	0.26
10	3.83	1.32
20	4.02	6.35
30	4.36	15.34

Table 7. Values for parameters A and B as a function of conductivity and Peclet number.

$\tilde{k}$	**Pe**	**A**	**B**
2	0.001	4.5687	3.5467
	0.005	5.2177	2.9293
	0.01	7.1143	1.4616
	0.05	13.4187	-7.0897
	0.1	16.0432	-9.0012
4	0.001	3.8590	5.9664
	0.005	4.7474	4.0799
	0.01	5.5838	2.8738
	0.05	11.038	-5.1873
	0.1	13.342	-6.0213
6	0.001	3.4670	8.7863
	0.005	4.0878	7.6578
	0.01	4.3378	6.1265
	0.05	7.8746	1.2389
	0.1	9.3269	0.6742
8	0.001	3.3320	11.715
	0.005	3.9910	10.141
	0.01	4.3967	9.7387
	0.05	6.3037	3.7139
	0.1	7.3866	3.2603

Table 8. Test case used for evaluation of required borefield length as a function of the ground parameters.

Variable	Value	Variable	Value
T_g	10°C	q_y	8 kW
T_{fm}	0°C	q_m	20 kW
r_b	0.075 m	q_h	30 kW
R_b	0.25 mK/W	N_x	5
τ_y	15 years	N_y	4
τ_m	2 months	B	4 m
τ_h	24 hours		

Figure captions

Figure 1 Schematic representation of the proposed H/TRT setup with groundwater flow.

Figure 2 Example of simulated temperature profile in and around the borehole after a day of heating (isotherms with a 2 K increment are shown).

Figure 3 Example of temperature evolution measured by sensors for a) Pe = 0.001 b) Pe = 0.01 c) Pe = 0.05 and d) Pe = 0.1. Each color represents a different sensor.

Figure 4 Example of the evolution of the differences of temperature between sensors for a) Pe = 0.001 b) Pe = 0.01 c) Pe = 0.05 and d) Pe = 0.1. Each color represents the difference of temperature between the probe installed at the warmest position and a different probe.

Figure 5 Schematic view of the borehole during the test to illustrate the definition of ΔT_{max}.

Figure 6 Maximum dimensionless difference of temperatures on the borehole wall versus the flow Peclet number.

Figure 7 Ground function for the TRT a) as a function of the Peclet number, and b) as a function of the ratio of thermal conductivities.

Figure 8 Suggested flowchart for the H/TRT analysis procedure.

Figure 9 Comparison between estimates of the parameters obtained from the H/TRT and their actual values for a series of random cases: a) subsurface thermal conductivity b) Darcy velocity c) flow orientation, and d) required borefield length. (Both values are equal when markers fall on the black dashed line. Red dashed lines correspond to an error of $\pm 10\%$).

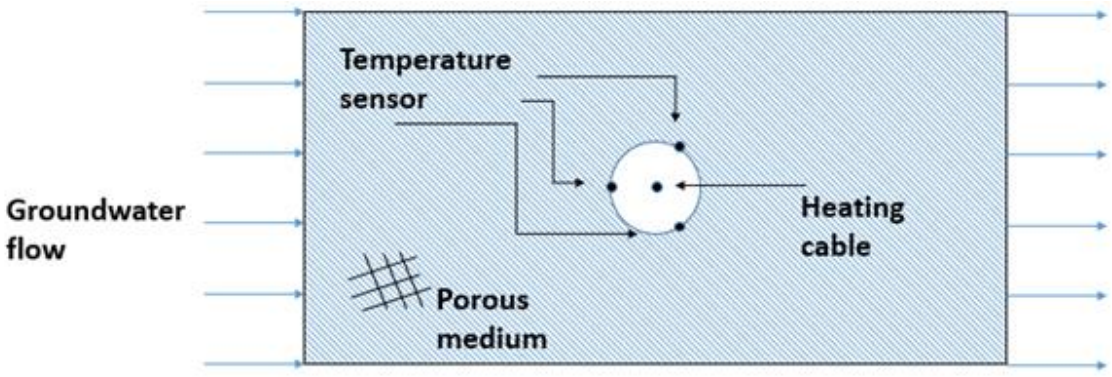
Temperature
sensor
Groundwater
flow
Heating
cable
Porous
medium

Figure 1

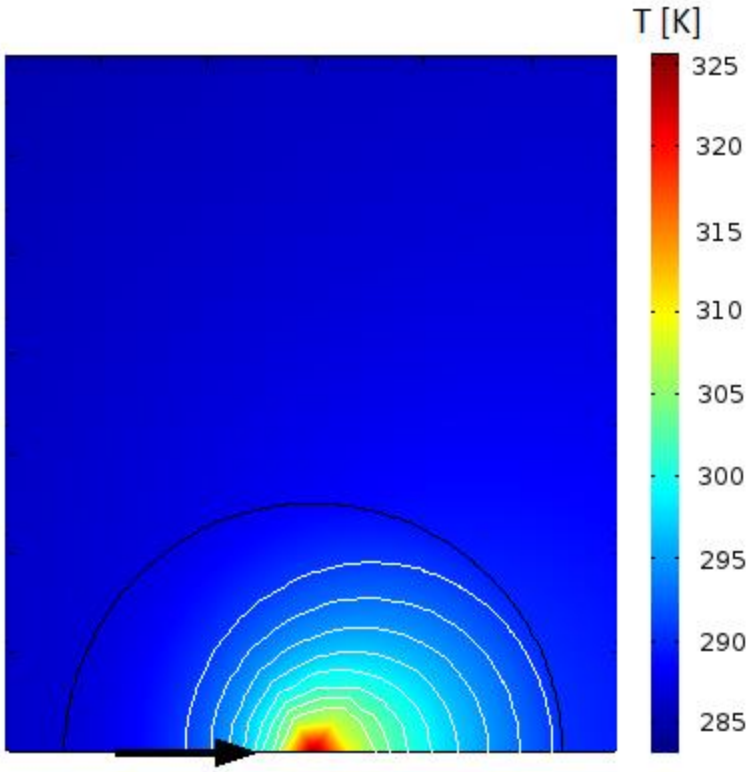

Figure 2

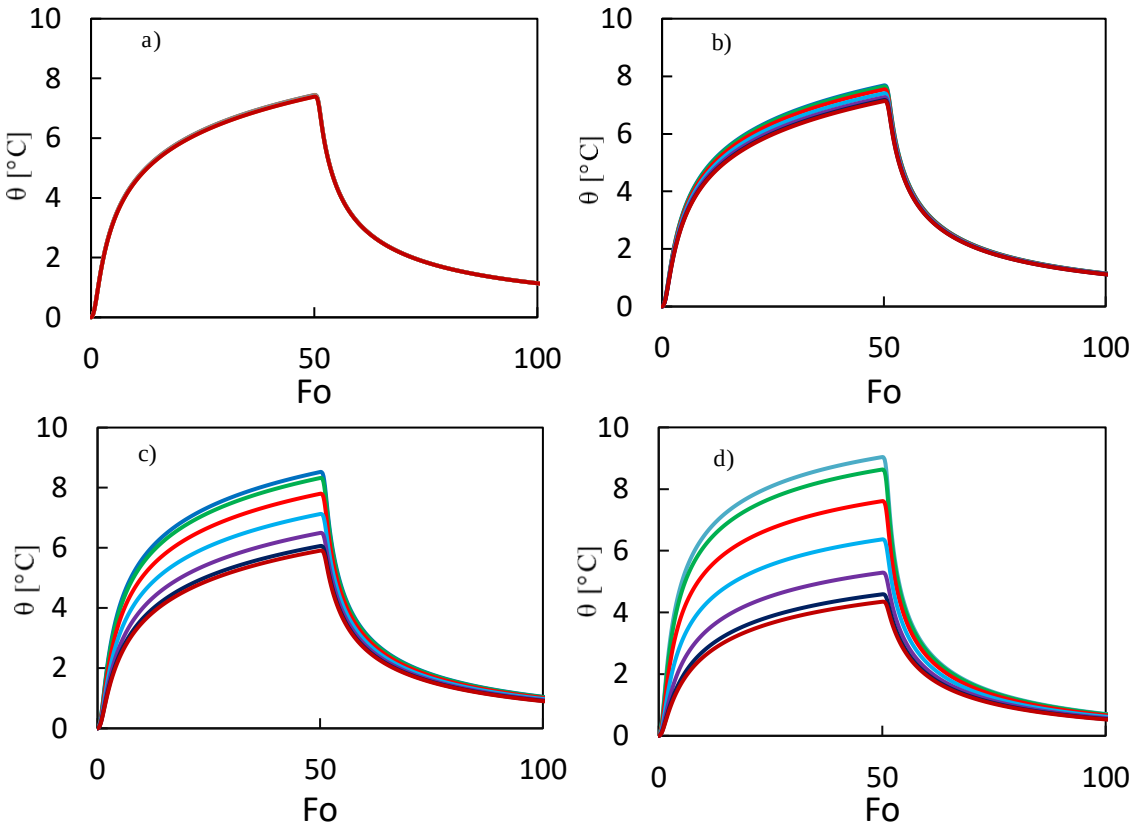

Figure 3

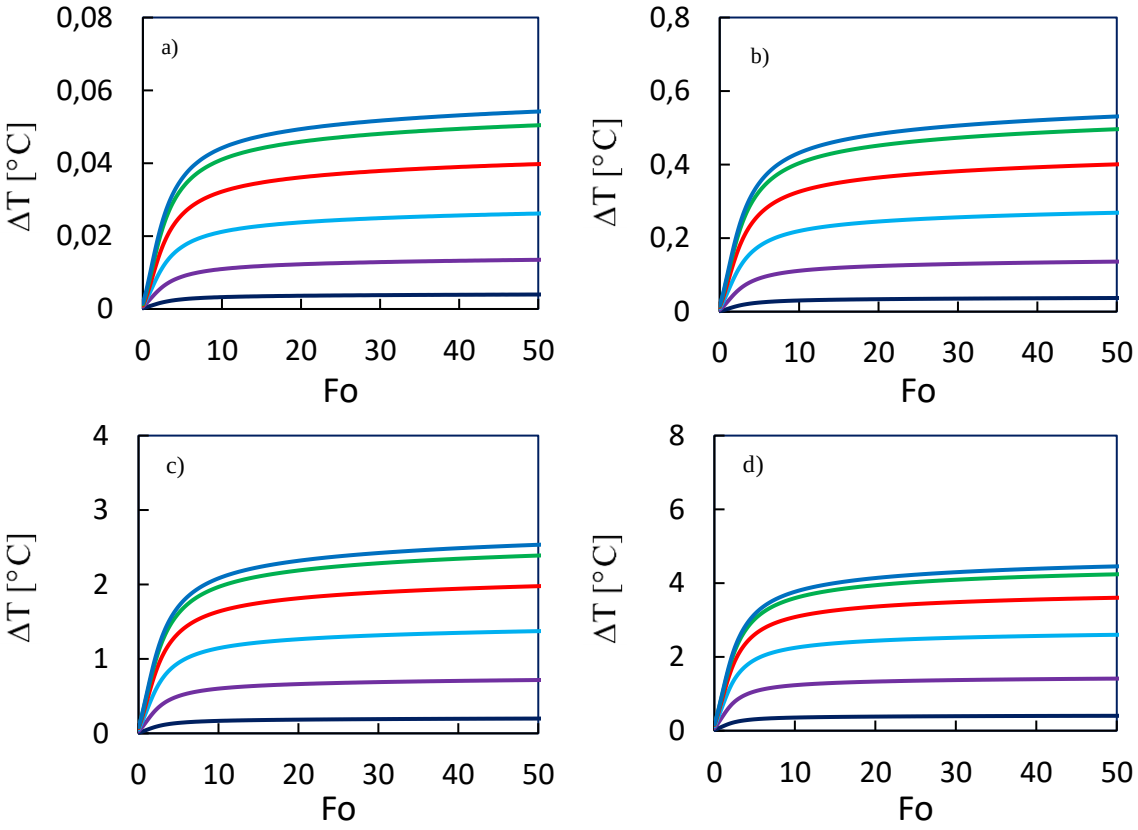

Figure 4

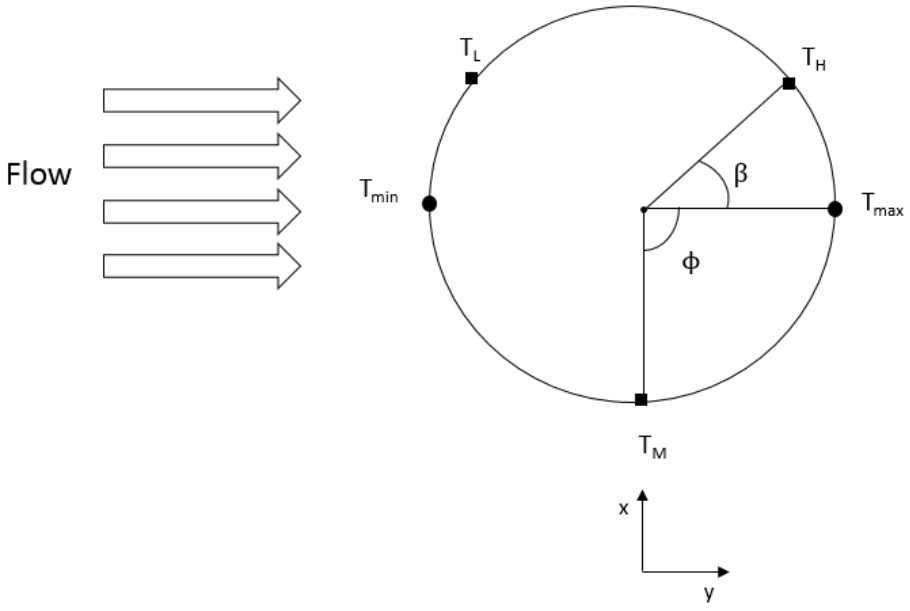

Figure 5

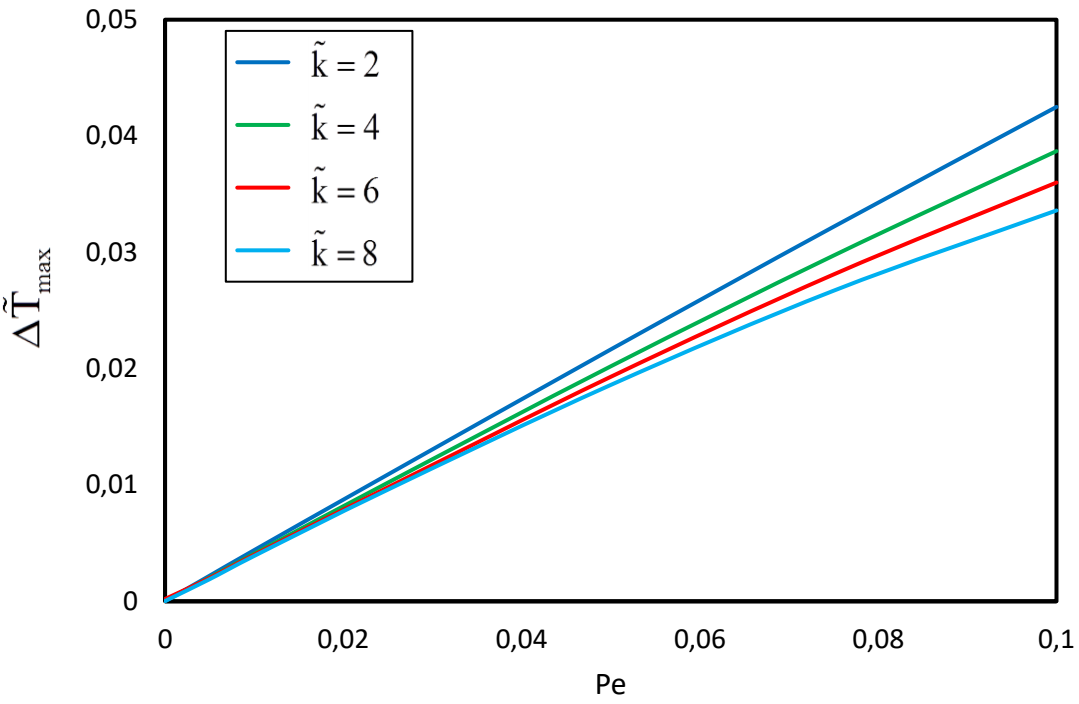
0,05
0,04
0,03
0,02
0,01
0
$\Delta\tilde{T}_{max}$
$\tilde{k} = 2$
$\tilde{k} = 4$
$\tilde{k} = 6$
$\tilde{k} = 8$
0
0,02
0,04
0,06
0,08
0,1
Pe

Figure 6

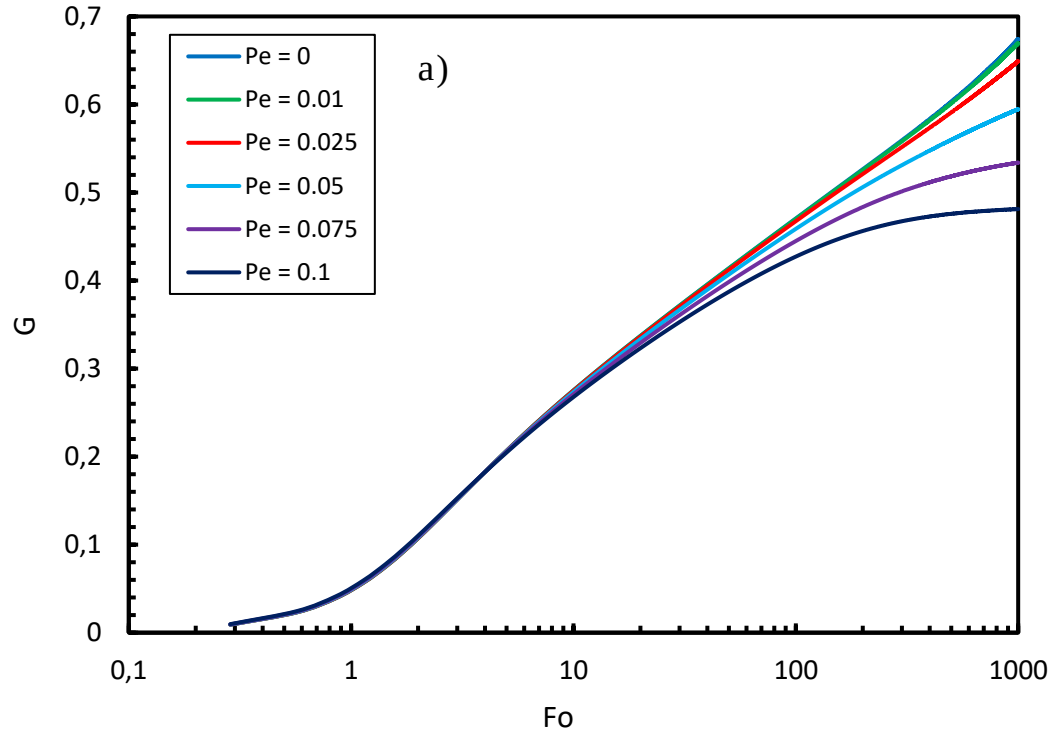
a)
Pe = 0
Pe = 0.01
Pe = 0.025
Pe = 0.05
Pe = 0.075
Pe = 0.1
G
Fo
0,7
0,6
0,5
0,4
0,3
0,2
0,1
0
0,1
1
10
100
1000

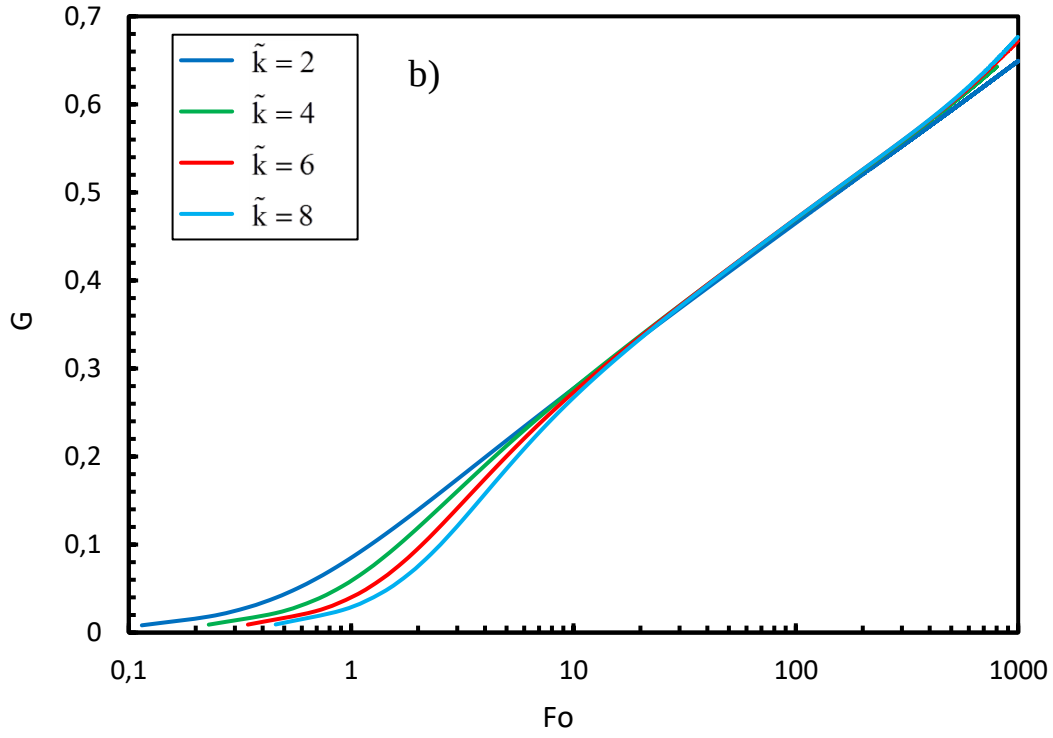
b)
$\tilde{k} = 2$
$\tilde{k} = 4$
$\tilde{k} = 6$
$\tilde{k} = 8$
G
Fo
0,7
0,6
0,5
0,4
0,3
0,2
0,1
0
0,1
1
10
100
1000

Figure 7

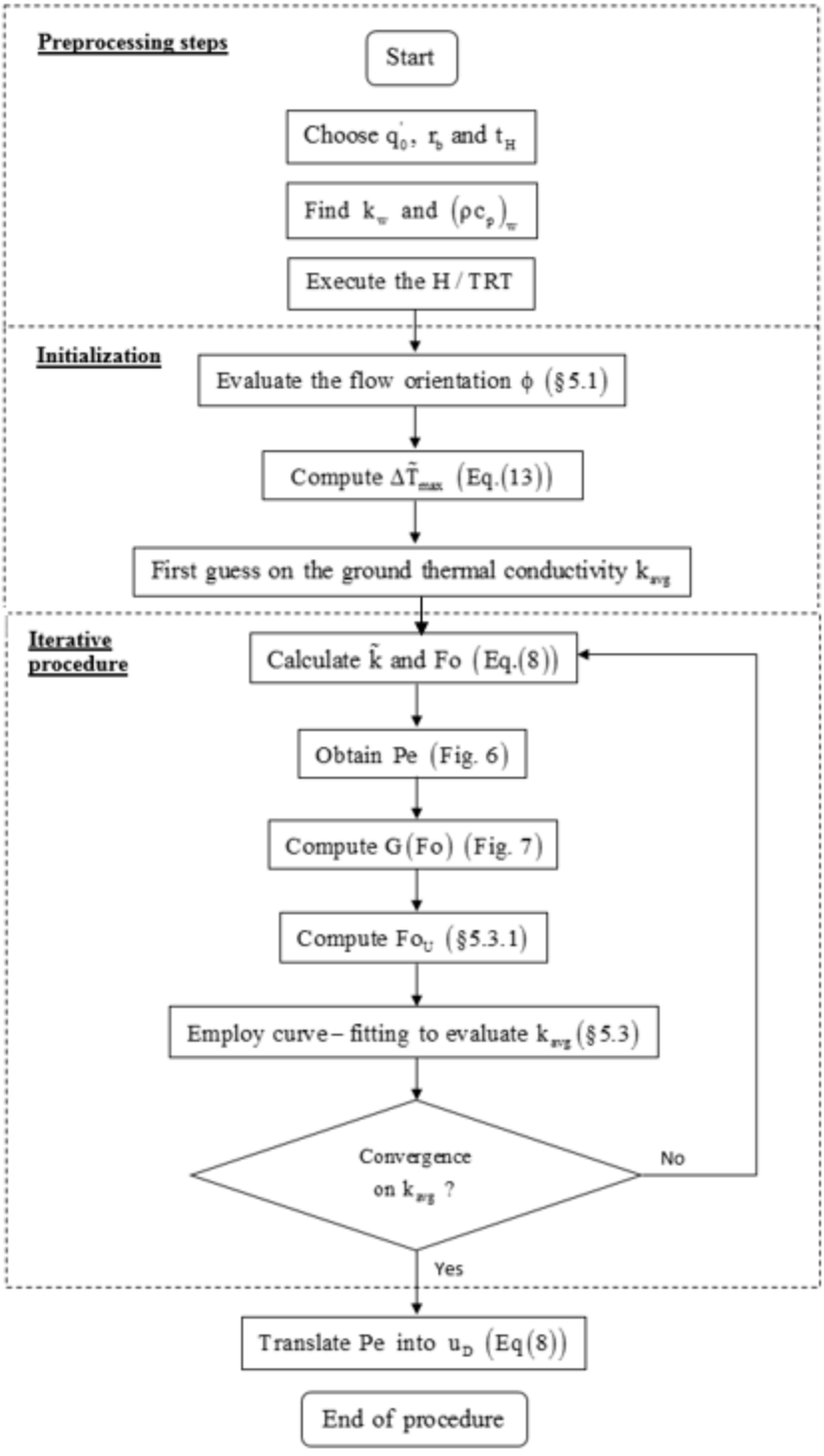
Preprocessing steps
Start
Choose q_0', r_b and t_H
Find k_w and $(\rho c_p)_w$
Execute the H / TRT
Initialization
Evaluate the flow orientation ϕ (§5.1)
Compute $\Delta\tilde{T}_{max}$ (Eq.(13))
First guess on the ground thermal conductivity k_{avg}
Iterative procedure
Calculate $\tilde{k}$ and Fo (Eq.(8))
Obtain Pe (Fig. 6)
Compute G(Fo) (Fig. 7)
Compute Fo_U (§5.3.1)
Employ curve – fitting to evaluate k_{avg} (§5.3)
Convergence on k_{avg} ?
No
Yes
Translate Pe into u_D (Eq(8))
End of procedure

Figure 8

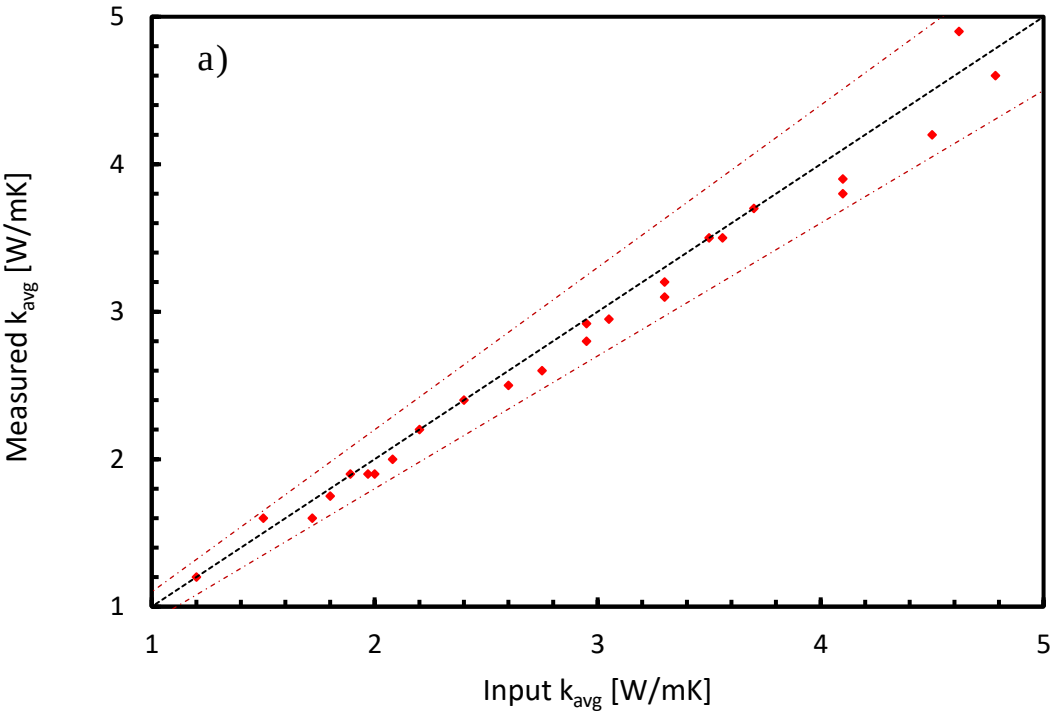
a)
Measured k_{avg} [W/mK]
Input k_{avg} [W/mK]
1
2
3
4
5

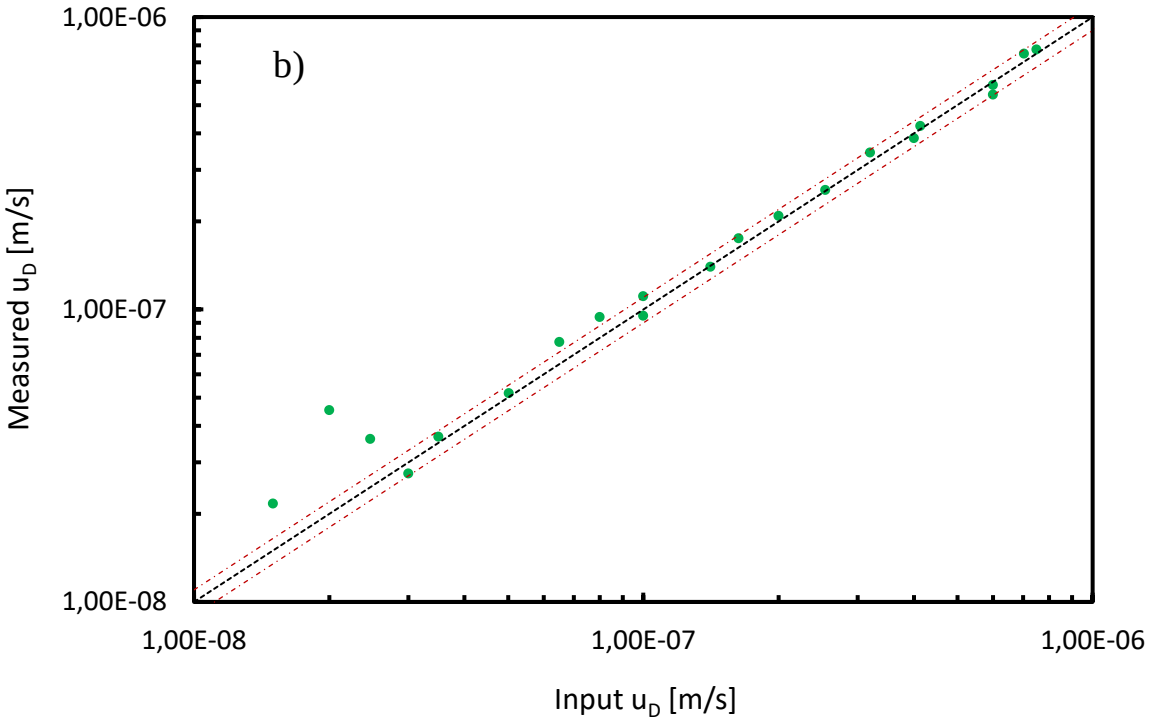
b)
Measured u_D [m/s]
Input u_D [m/s]
1,00E-08
1,00E-07
1,00E-06

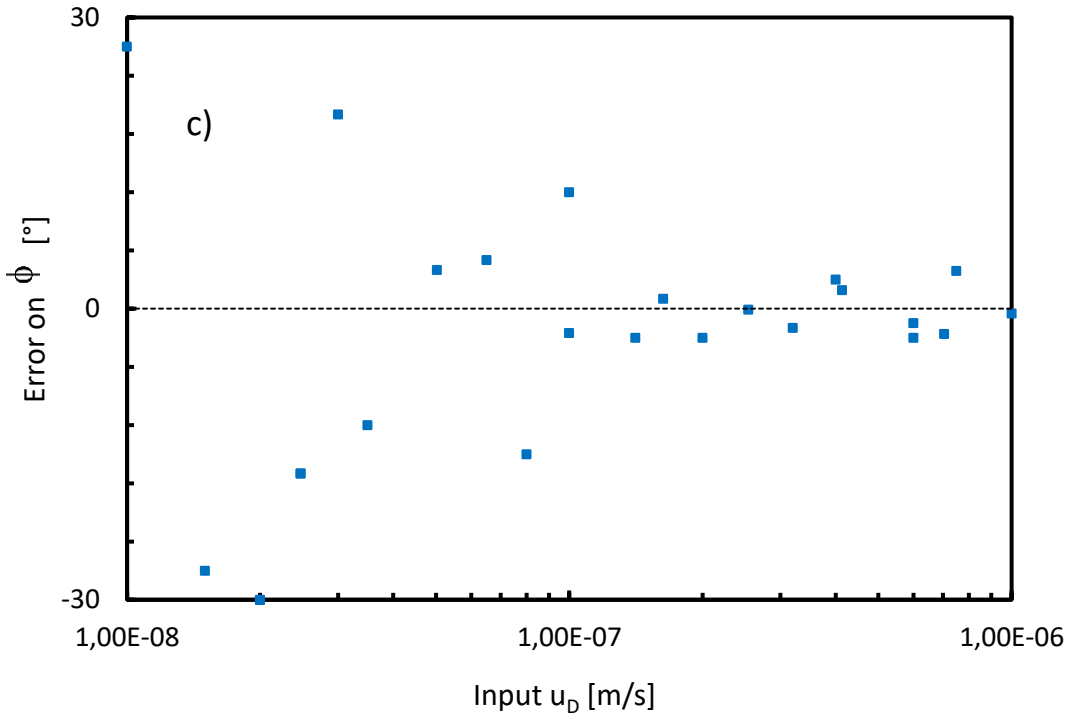
c)
30
0
-30
Error on ϕ [°]
1,00E-08
1,00E-07
1,00E-06
Input u_D [m/s]

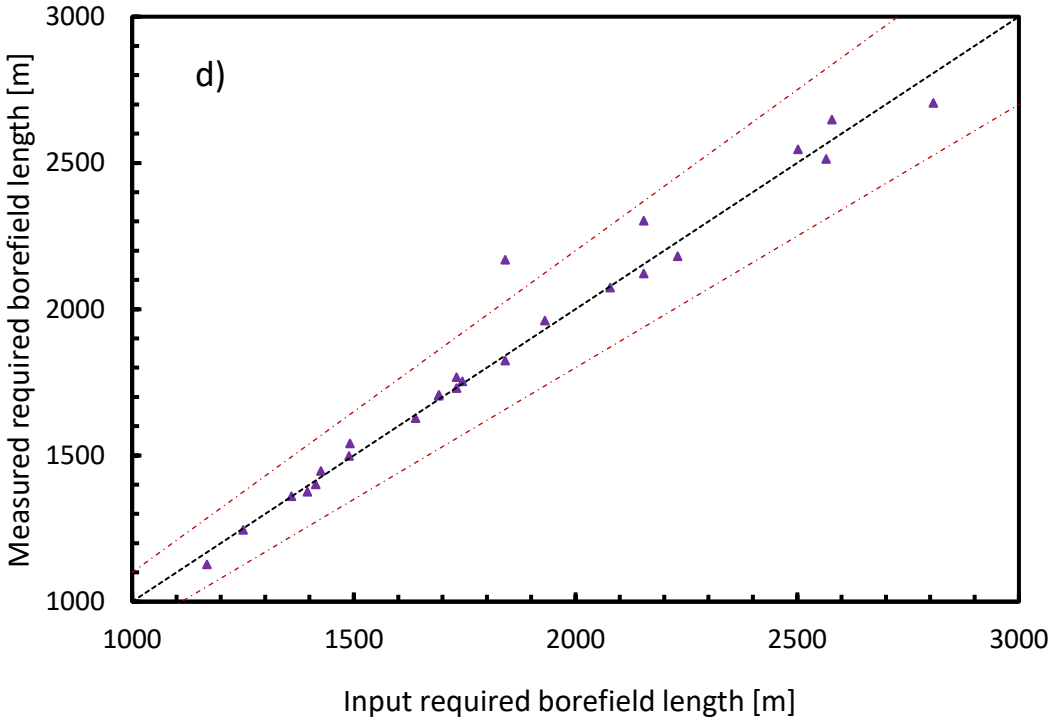
d)
3000
2500
2000
1500
1000
Measured required borefield length [m]
1000
1500
2000
2500
3000
Input required borefield length [m]

Figure 9